Influences on the Dynamics and Stability of Self-Assembly: Solvent, Substrate, and Concentration

*Kirill Gurdumov, Ursula Mazur, and K.W. Hipps**

Department of Chemistry and Materials Science and Engineering Program, Washington State University, Pullman, Washington 99163-4630, United State

Corresponding Author: hipps@wsu.edu

ABSTRACT

The formation dynamics and stability of CoOEP at the solution/Au(111) interface is captured in-situ using scanning tunneling microscopy (STM) in a dynamic solution flow cell at room temperature. The intermediate steps of self-assembly of CoOEP into an ordered monolayer were captured and fractional coverage as a function of time was measured to extract characteristic parameters of the self-assembly process. Adlayer structure and formation under various solvents is compared to previous studies conducted on HOPG. The choice of substrate is found to have a dramatic influence on adlayer structure and stability. It was found that the CoOEP adlayer assembly on HOPG is an equilibrium process and the monolayer can be readily formed within minutes of contact with solution (above a solvent-dependent threshold solution concentration), and the dissolution of the formed adlayer is feasible, though the rate of dissolution is solvent-dependent. The assembly of an adlayer on Au(111) is kinetically driven, monolayer formation occurs within minutes, and dissolution is very slow -- only minimal island dissolution was achieved after hours of pure solvent flow.

Solvent incorporation of 1,2,4-trichlorobenzene (TCB) was observed to form a CoOEP pseudo-rectangular adlayer structure (REC) on both HOPG and Au(111), though a solvent-free pseudo-hexagonal structure (HEX) occurred at much higher concentrations of CoOEP on HOPG than on Au(111). This is likely due to the fact that CoOEP binds more strongly to Au(111) than HOPG, which promotes the REC to HEX transition on Au(111) at lower concentrations. Solvent incorporation of toluene (Tol) into a CoOEP adlayer on Au(111) was observed, but it did not incorporate into the adlayer on HOPG. There is a significant increase in the Arrhenius desorption rate factor (~350) of toluene on HOPG relative to Au that is likely a driving factor for Tol co-

adsorption on Au. A very short-lived decane incorporated adlayer was also observed. The transformation on Au(111) from REC to HEX structure under 1 μM CoOEP in Tol occurred within ~10 minutes, while under a solution of 470 μM CoOEP in TCB the transformation required ~10^2 minutes. This variance is primarily due to the relative residence times of the solvent molecule on the Au(111) surface, where Tol has an estimated desorption rate 500 times greater than TCB. The unit cells of the CoOEP adlayer are also substrate dependent. The commensurate TCB-incorporated REC structure on Au(111) contains two CoOEP but only one CoOEP on HOPG. Thus, the adlayer formation of CoOEP on Au(111) was more significantly affected by solvent than for adsorption on HOPG.

KEYWORDS: self-assembly, formation dynamics, scanning tunneling microscopy, solution/solid interface

INTRODUCTION:

Formation of thin films at the solution/solid interface can produce pristine arrays of molecular layers spanning large distances. Non-covalent self-assembly, driven by 'weak' intermolecular interactions, allows for versatility in thin film formation.[1] A model for non-covalent self-assembly at the solution/solid interface has been proposed in which a solution of tectons (or building blocks) are brought into contact with a solid support and an ordered adlayer spontaneously forms.[2] Further, the importance of solvent desorption in the initial tecton adsorption and the subsequent self-assembled monolayer (SAM) formation has recently been quantitatively demonstrated.[3] Solvent influence and control in self-assembly have been studied in various systems.[4,5,6] Depending on the delicate balance of tecton-solvent, tecton-tecton, solvent-solvent, tecton-substrate, and substrate-solvent interactions, competitive deposition of solvent with adsorbate is possible.[6] This could

result in solvent-incorporation into an adlayer, phase segregation, or preferential solvent adsorption that prevents the assembly of an ordered tecton adlayer. Typical solvents observed to co-adsorb have been long alkyl chains,[7,8] hydrogen-bond donors or acceptors,[9-13] or a combination of moieties.[14-16]

Scanning tunneling microscopy (STM) is an ideal tool for studying SAMs because it provides sub-molecular resolution and can be used in a wide range of environments. STM can be performed on any conducting surface in UHV[17], gaseous atmosphere[18], conducting[19] or non-conducting[20] solution. Many of the STM studies of non-covalent self-assembly have focused on systems with tectons containing long alkyl chains or acidic moieties to enhance SAM stability and as a design parameter. These substituents act via weak interactions (e.g., van der Waals, dipole-dipole, or hydrogen bonding). STM has also been used to investigate the effects halogen interaction in the self-assembly process,[21-23] both in cases of halogenated tectons and of halogenated solvents.

In this study, we focus on the effects of solvent and substrate on the structure, stability, and dynamics of a physisorbed porphyrin SAM. Decane (Dec), 1-phenyloctane (PhO), toluene (Tol), and 1,2,4-trichlorobenzene (TCB) are the solvents considered (Figure 1). The results on Au(111) reported here are compared to previous work on HOPG[20]. A dense pseudo-hexagonal SAM structure is formed when solvents PhO and Dec are used. In the case of TCB and Tol, a combination of factors to be identified later results in the formation of solvent-incorporated psuedopolymorphs. Adsorption energies were calculated for each solvent molecule. The intermediate steps of self-assembly of porphyrin into an ordered monolayer were captured and fractional coverage as a function of time was measured to extract characteristic parameters of the self-assembly process.

This study exemplifies the importance of both the substrate and solvent in determining the structure and stability of a given SAM. While there have been many studies of the role of solvent on self-assembly on graphite, comparison of the role of the substrate is rare.

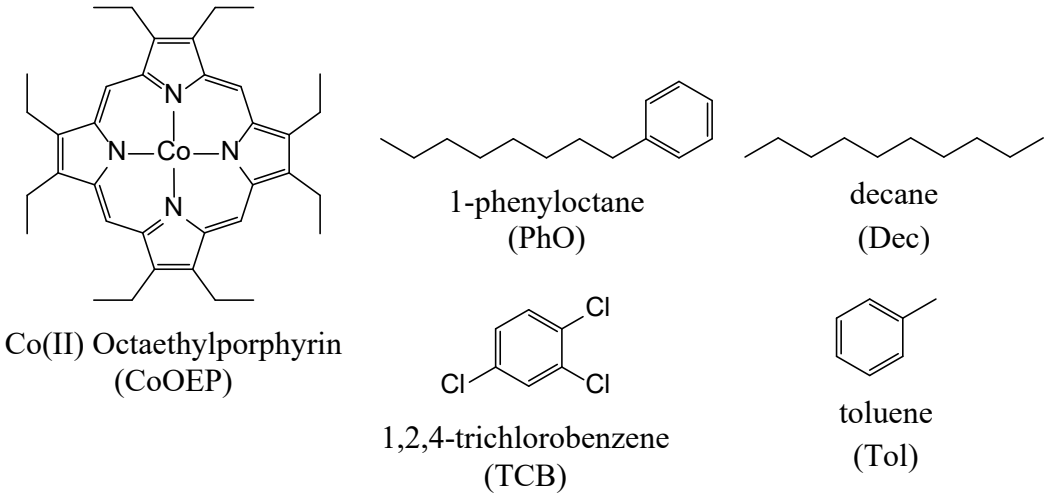

Figure 1. Chemical structure of materials used in this study.

EXPERIMENTAL AND THEORETICAL METHODS

Materials. 2,3,7,8,12,13,17,18-Octaethyl-21H,23H-porphine cobalt(II) (CoOEP) was purchased from Aldrich. 1,2,4-trichlorobenzene (≥99%, Sigma-Aldrich%), 1-phenyloctane (≥98%, TCI), toluene (≥99.7%, J.T. Baker), decane (≥99%, Alfa Aesar). All reagents were used without further purification. STM tips were prepared by mechanically cutting $Pt_{0.8}Ir_{0.2}$ wire (0.010-inch diameter, California Fine Wire Company). Au(111) surfaces were prepared by hydrogen flame annealing freshly deposited gold on mica substrate, and imaged to confirm distinct reconstruction lines.

STM Experiment. Self-assembly of CoOEP at the solution/HOPG interface was monitored via a commercial scanning tunneling microscopy (STM) [Molecular Imaging PicoPlus]. Constant current imaging was used throughout, and the set-point conditions are indicated in figures and/or captions. All STM images were plane corrected and lightly filtered using Scanning Probe Imaging

Processor (SPIP) software (Image Metrology A/S). The sample cell was designed and built specifically for this work and will be described below.

Measurements of unit cell parameters were averages from drift corrected images. The STM was routinely calibrated by imaging the HOPG lattice. No aldayer structure was observed when pure solvents were deposited onto the Au(111) substrate. Fresh solutions of CoOEP in a given solvent were prepared before each set of experiments. Samples were made by dissolving a small amount of CoOEP solid in a few mL of solvent, and then determining the concentrations using UV-VIS spectroscopy and the known adsorption coefficients: 1.53×10^5 $cm^{-1}M^{-1}$ (Dec), 2.18×10^5 $cm^{-1}M^{-1}$ (PhO), 2.16×10^5 $cm^{-1}M^{-1}$ (Tol), 2.63×10^5 $cm^{-1}M^{-1}$ (TCB). The absorption coefficient values were determined by dividing the absorption value of the Soret band (near 420 nm) by the known concentration of a carefully prepared porphyrin solution in a given solvent. These stock solutions were then diluted to the appropriate concentrations needed for the given experiment. A custom Teflon solution flow cell (55 µL volume) with stainless steel inlet and outlet was designed to allow for the dynamic control of solution during STM experiments. A Kalrez O-ring was used to make a seal between the cell and sample. A mechanical syringe pump (Harvard Apparatus Ecoflo) was used to transport solution through Teflon tubing to the STM flow cell (55 µL/min), while a second syringe pump (Harvard Apparatus Pump 11 Pico Plus Elite) was used to withdraw solution to hold a constant volume within the flow cell. Flow rate was decreased to 5 µL/min after one minute of 55 µL/min flow rate. Experimental setup shown in Figure 2. A scale diagram of flow cell (Figure S1) and photo of flow cell assembled with STM stage (Figure S2) can be found in the SI.

The flux of the solution (flow rate times concentration) is an important parameter of these experiments. If the system was not properly isolated, mechanical noise would propagate through the flow of solution and interfere with the STM imaging, causing significant drift or noise. If the

flow was halted upon the first observation of island nucleation, incomplete monolayer growth was typically observed. The quantitative effects of the flow rate on the dynamics of growth should be further studied to remove any possible artifacts due to flow in the nucleation and growth parameters.

The approximate solubility limit near room temperature of CoOEP in each solvent varied drastically: 7 mM in TCB, 0.8 mM in Tol, 0.2 mM in PhO, 0.04 mM in Dec. This was determined by preparing a saturated solution of CoOEP in ~5 mL of solvent while continuously stirring. The concentration of the supernatant solution was determined using the compound's adsorption coefficient (above) in each solvent. However, most of the reported solutions used for these STM studies were well below the solubility limit.

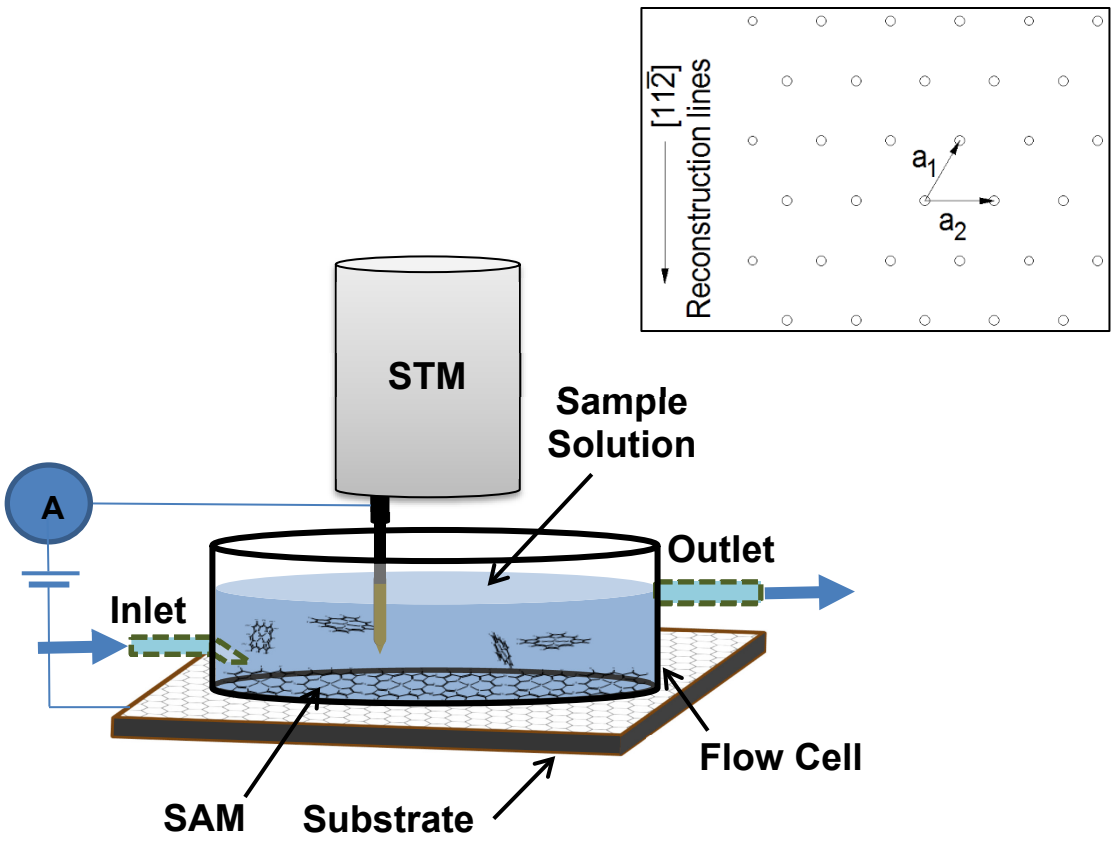

Figure 2. Experimental setup of STM and flow cell. Solution is driven into flow cell with a mechanical pump through inlet, and a syringe pump pulls excess solution from outlet. Diagram of Au(111) lattice and unit cell vectors ($\mathbf{a}_1$, $\mathbf{a}_2$).

UV-Visible Absorption Spectroscopy. All spectra were acquired using an Evolution 260 Bio spectrophotometer (Thermo Scientific, Waltham, MA, USA) with a 0.1 cm path length quartz cuvette from 300 nm to 700 nm. Stock solutions of CoOEP were made by dissolving a small amount of solid in each solvent, measuring the absorption spectrum, and calculating the concentration using a previously determined extinction coefficient of the Soret band near 400 nm. Appropriate dilutions were made from these stock solutions for each experiment.

Computational Methods. Computations are performed with density functional theory (DFT) using Vienna Ab-initio Simulation Package (VASP)[24,25] version 6.2.0. The VASP code uses the projector augmented wave (PAW) method[26,27] to describe the core electrons and valence–core

interactions. We used the optB88-vdW functional[28,29] with PAW potentials optimized for the PBE functional[30] for all calculations. The electronic wavefunctions were determined at the Gamma (Γ) point in the irreducible Brillouin zone (BZ). A plane wave cut off energy of 550 eV was used for all simulations. For the Au(111) and adsorbate-Au(111) systems, Methfessel–Paxton smearing was used to set the partial occupancies for each wave function with a smearing width of 0.2 eV. For the isolated molecular systems Gaussian smearing was used with a width of 0.04 eV. All the geometries were fully optimized up to 0.001 eV energy convergence. The choice of our DFT methodology, plane wave cutoff energies and k-point choice were based on previous periodic DFT simulations of similar systems of type[31-35] and size.[36] VASP calculations were performed on species adsorbed to 3-layer unreconstructed Au and on the same species in the gas phase. Only the top layer of Au was allowed to vary in position during adsorption optimization.

RESULTS AND DISCUSSION

Adlayer Structure.

CoOEP was observed to form stabile adlayers on Au(111) at 22˚C from solvents 1,2,4-trichlorobenzene (TCB), toluene (Tol), 1-phenyloctane (PhO), and decane (Dec). A pseudo-hexagonal adlayer structure (HEX) is the equilibrium structure formed under PhO and Dec (Figure 3) at all concentrations of CoOEP in the range from 0.05 μM up to the solubility limit in each solvent (noted under STM Experiment section above). The experimental lattice parameters for these structures are shown in Table 1. The commensurate lattice structures were determined by measuring the adlayer packing structures from several drift corrected experimental STM images. The relative angle (φ) between the adlayer unit cell vector (b) and the $[11\bar{2}]$ direction (parallel to reconstruction lines[37]) of the underlying Au(111) terrace was used as an orientation reference (±

3°) for determining the commensurate unit cell parameters. The lengths and interior angles were then chosen to make the unit cell vectors integer multiples of the underlying gold unit cell (assuming Au(111) instead of reconstructed Au(111) 22x√3). In terms of the underlying lattice vectors ($\mathbf{a}_1$, $\mathbf{a}_2$), the HEX unit cell is $\mathbf{a_h} = 10\mathbf{a}_1 + \mathbf{a}_2$ and $\mathbf{b_h} = 5\mathbf{a}_2$ (Figure 4). This structure contains two CoOEP molecules per unit cell, which agrees with previous observations of porphyrin adlayer on Au(111) with resolved ethyl groups under UHV.[38] A comparison of the HEX structure formed under Tol and under TCB is presented in Figure S3.

When deposited from TCB or Tol, pseudo-rectangular structures (Figure 3a & c) are initially formed (REC). The measured lattice parameters and the assigned commensurate lattice parameters for this structure are also presented in Table 1. In terms of the underlying lattice vectors, $\mathbf{a_r} = 10\mathbf{a}_1 + \mathbf{a}_2$ and $\mathbf{b_r} = 3\mathbf{a}_1 - 6\mathbf{a}_2$ for REC (Figure 4).

The lattice parameters of the observed adlayers under the various solvents on HOPG[20] are also presented in Table 1. Note that both HEX and REC structures on Au(111) contain two CoOEP molecules per unit cell, while on HOPG the HEX contains two and the REC just one CoOEP molecule per unit cell. The calculated areas of both structures (per CoOEP molecule) are slightly larger on Au(111) than on HOPG: 1.80 nm^2 vs. 1.74 nm^2 (HEX), 2.27 nm^2 vs. 2.21 nm^2 (REC). This suggests that the adlayer assemblies on HOPG are interacting more strongly laterally than on Au(111).

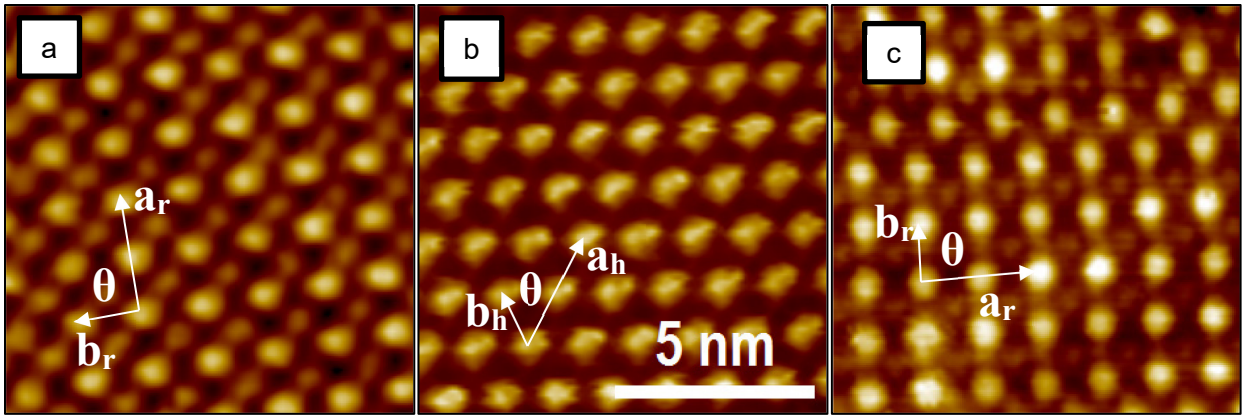

Figure 3. Representative STM images of observed adlayer structures of CoOEP on Au(111): REC under TCB (a), HEX under PhO, Dec, Tol, TCB (b), and REC under Tol (c). All images have equal scale. Note that the solvent-incorporated REC structures were observed to transition into the solvent-free HEX structure (~10^1 minutes under 1 μM Tol, ~10^2 minutes under 470 μM TCB). Scanning parameters: -0.4 V, 15 pA.

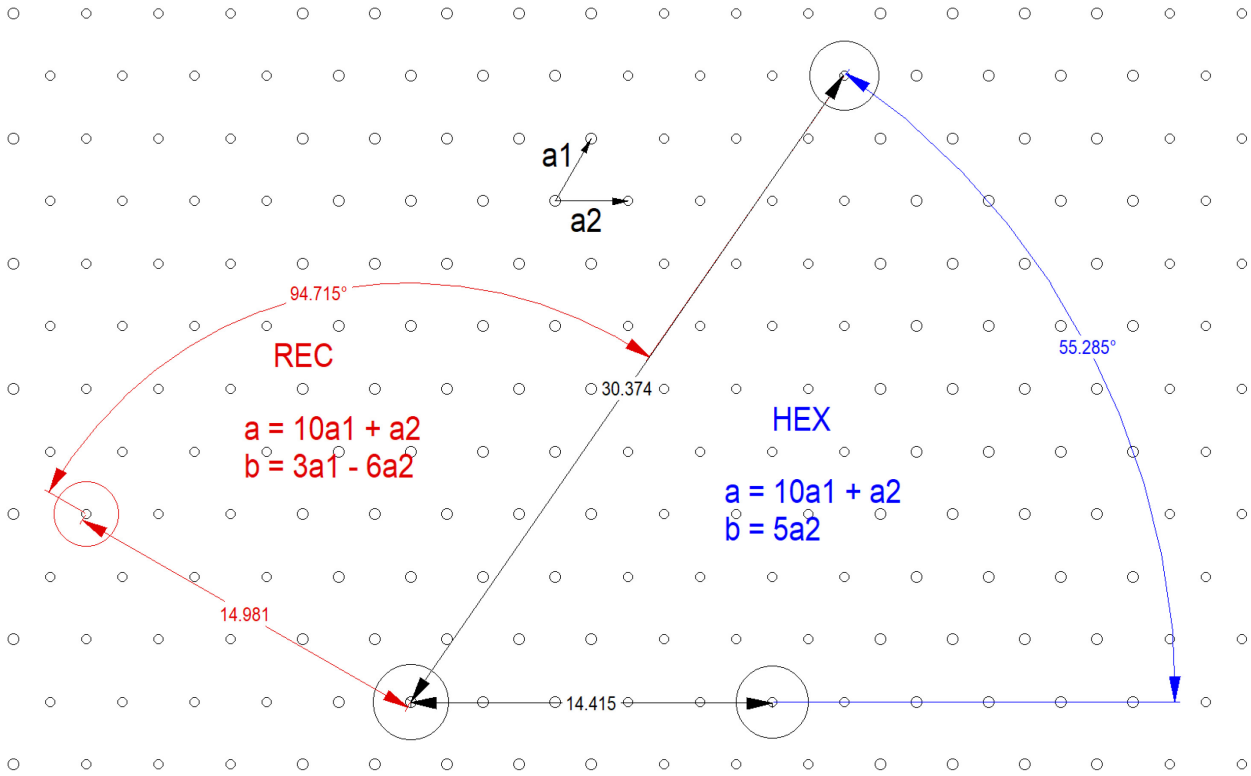

Figure 4. Commensurate structures of CoOEP on Au(111) under a solvents TCB (REC), Tol (REC), PhO (HEX), and Dec (HEX). Lattice vectors of substrate indicated by a1 and a2.

Table 1. Calculated commensurate and measured experimental unit cells of CoOEP adlayer deposited from respective solvents on substrates Au(111) and HOPG[20]. The relative angle (φ) between the adlayer unit cell vector (b) and the $[11\bar{2}]$ direction for Au(111) and the $[11\bar{2}0]$ direction for HOPG. Uncertainty in measured angles from experiment is ± 3.0°.

	Commensurate Unit Cell					Experimental Unit Cell			
					Au(111)				
Structure	a (nm)	b (nm)	θ (°)	φ (°)	Solvent	a (nm)	b (nm)	θ (°)	φ (°)
HEX[a]	3.04	1.44	55.3	90.0	PhO	2.99 ± 0.04	1.44 ± 0.03	56.8	87.6
					Dec	3.06 ± 0.02	1.43 ± 0.04	56.6	87.1
					Tol	3.06 ± 0.03	1.43 ± 0.03	56.4	89.0
					TCB	3.01 ± 0.02	1.41 ± 0.02	56.0	89.1
REC[a]	3.04	1.50	85.3	60.0	Tol	2.94 ± 0.05	1.44 ± 0.02	89.5	59.1
					TCB	3.04 ± 0.02	1.48 ± 0.02	88.4	59.1
					HOPG				
HEX[a]	1.48	2.71	60	30	PhO	1.49 ± 0.05	2.68 ± 0.06	57.8	29.4
					Dec	1.52 ± 0.03	2.76 ± 0.03	57.9	26.9
					Tol	1.50 ± 0.03	2.74 ± 0.04	58.5	26.5
					TCB	1.50 ± 0.02	2.70 ± 0.02	58.0	28.0
REC[b]	1.48	1.50	85.3	4.7	TCB	1.47 ± 0.04	1.50 ± 0.02	88.1	6.5

[a] 2 CoOEP/unit cell

[b] 1 CoOEP/unit cell

At low concentrations in Dec (<0.5 μM), a transient rectangular structure is observed. The measured unit cell was found to be **a** = 2.30 nm (±0.02), **b** = 1.38 nm (±0.02), θ = 99.7° (±3). The angle between **b** and the reconstruction lines was 90° (±3). The commensurate unit cell for this structure was not determined. It is not clear if this structure is driven by decane solvent incorporation. A similar transient structure was observed with ZnOEP at the tetradecane/HOPG interface.[39] Even though several studies which show alkanes forming monolayers on Au(111)[40-43], an ordered decane adlayer was not observed in the present study, performed at 295 ± 1 K. This

is consistent with the reported decane monolayer 'melting' point on Au(111) of 292 ± 1 K[40]. It is also unlikely that a porphyrin overlayer is forming on top of a decane layer, especially since the measured unit cell structure of the HEX system on Au(111) in decane is the same as the HEX system in the other solvents (within uncertainty). Kim *et al*[43] observed a proposed porphyrin-overlayer on octanoic acid solvent, though the kind of bilayer features presented were not observed in our system of study. Thus, we discount the possibility that the CoOEP is forming on decane rather than directly on Au.

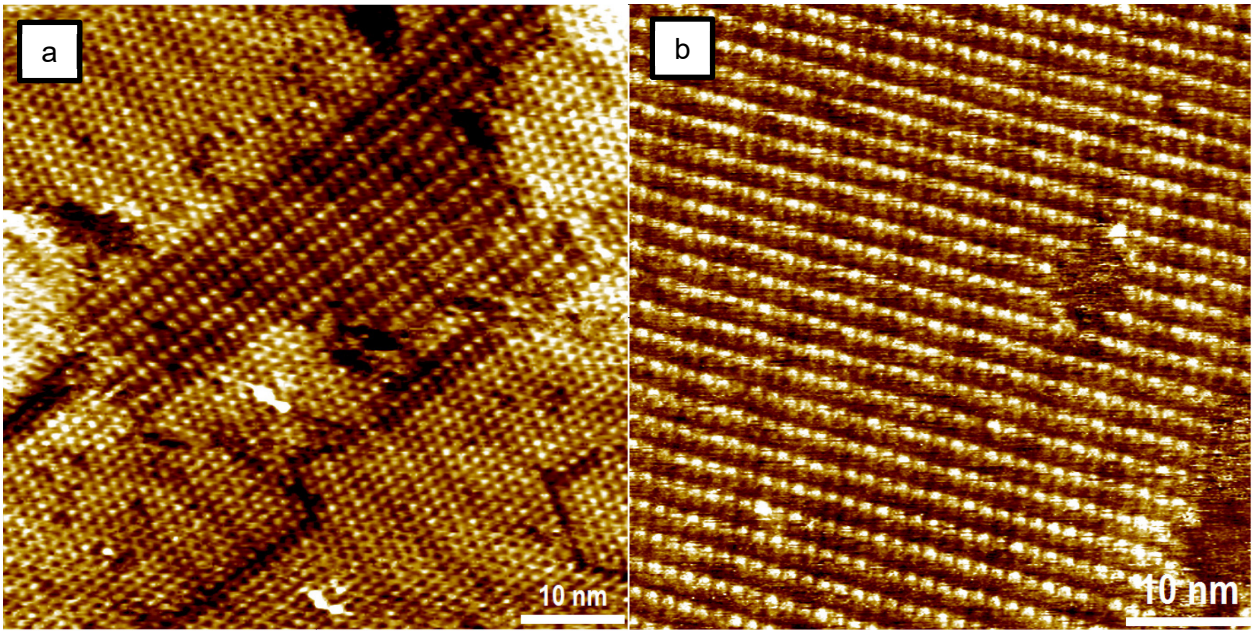

Figure 5. Images of transient rectangular structure at low concentrations (<0.5 μM CoOEP in Dec). (a) Rectangular structure surrounded by HEX grains. (b) large grain of rectangular structure. Scanning parameters: -0.4 V, 20 pA.

The images of the Tol and TCB REC systems in Figure 3 clearly show some additional electronic density in the region between the CoOEP. Because the lattice structures are too big for a single porphyrin per unit cell but too small for two, we assign this excess electronic density to incorporated solvent, where the benzene core is resolved but not the methyl group (for Tol) or the chlorines (for TCB). Similar resolution of TCB was observed in other host-guest surface studies.[44-

[48] To date, no other studies were found to have reported observations of toluene solvent incorporation into a self-assembled adlayer.

When the CoOEP began to outcompete with the solvent for surface sites, a coexistence of both the REC and HEX structures was observed (Figure 6). Under Tol, this occurred when an adlayer was formed from solution with concentrations of 1 μM CoOEP. When the concentration was increased to 10 μM, only the HEX structure was observed. Under TCB, it wasn't until high concentrations of 470 μM CoOEP were present that both structures were observed to coexist. Even at concentrations near the saturation limit in TCB (~7 mM), grains of both REC and HEX were observed in a newly formed adlayer. Thus, we identify the REC structures as pseudopolymorphs[49] (of the solvent-free HEX structure). When comparing CPK models of the HEX structure and a Tol molecule, it is clear that there is no space for solvent incorporation (see Figure S4). Mutual grain boundaries between the REC and HEX structures shared unit cell directions: HEX(**a**) with REC(**a**). Even with an average STM tip, it is easy to differentiate the REC and HEX grains because of the distinct contrast difference due to the nearly 20% difference in molecular packing density. This is the first observation of Tol incorporation into a self-assembled adlayer to be reported. Wang et al[50] reported polymorphism of a $CuPcOC_8$ deposited from toluene onto HOPG but did not report solvent incorporation. They attributed the difference between the two observed structures as due to a thermodynamically stabile state (hexagonal phase) and a kinetically favorable but thermodynamically metastable state (quartic phase). Kim et al[43] reported on the restructuring of a mixed adlayer of H_2OEP and CoOEP at the octanoic acid/Au(111) interface, where they observed a transition from a metastable 'parallel' phase (with a rectangular unit cell) to a hexagonal phase. They assigned this rectangular structure to the porphyrin assembling atop of a layer of solvent.

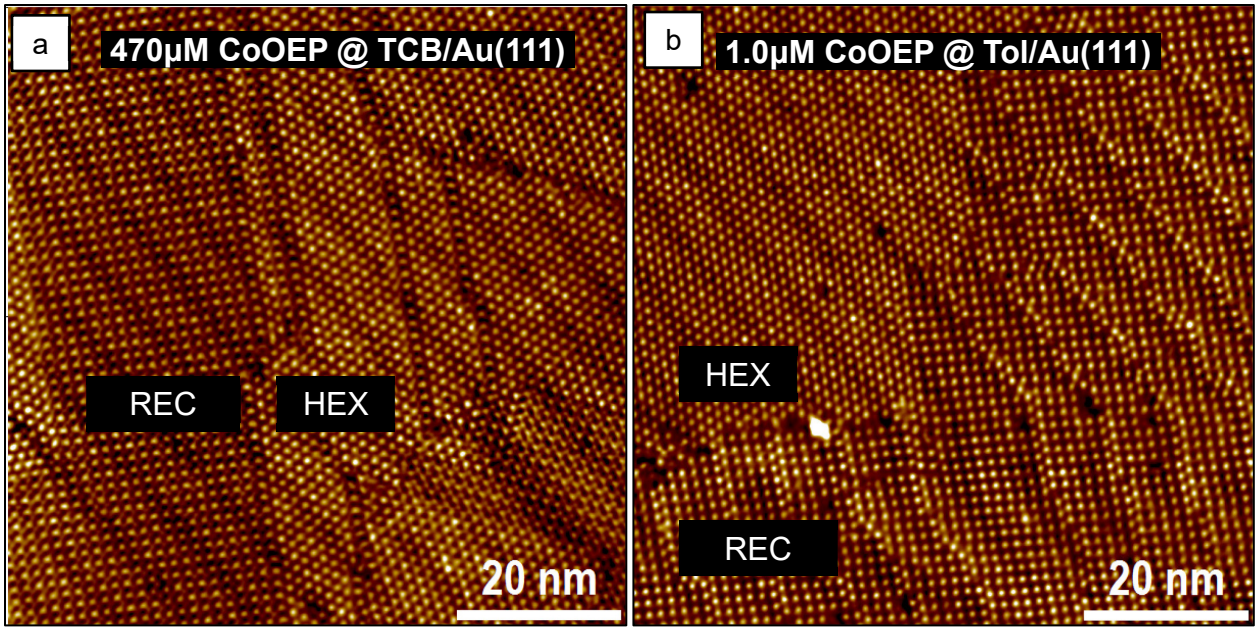

Figure 6. Coexistence of pseudopolymorphs REC and HEX structures of CoOEP on Au(111) under TCB (a) and Tol (b). Au(111) reconstruction lines can be seen under adlayer. Scanning parameters: -0.4 V, 15 pA.

At 1 μM in Tol, a complete transformation of REC monolayer into HEX occurred on the order of ~10 minutes, an example of the time sequence of transformation is shown in Figure 7 (a-c). This phase transition was accelerated by defects at grain boundaries. The REC_{TCB} phase was also observed to transition into the HEX structure over a much longer time period (~10^2), but only when extremely high concentrations of CoOEP were present in solution (~500 μM). An example of this transformation is shown in Figure 7 (d-f). The resilience of the REC structure is indicative of an energetically stabile, solvent-incorporated adlayer and reflects the strength of interaction between TCB and the Au(111) substrate, as well as between TCB and CoOEP through Cl-H bonding. Note that the 470 μM concentration solution in TCB was left static and not flowing. The concentration was such that gradients due to diffusion were not observed.

The nature of the reconstruction lines of the Au(111) substrate effected the grain size and dynamics of the adlayer structure. Under all solvents, areas of many grain boundaries with smaller grains were often observed atop of the herringbone elbows of the reconstructed surface. Under

Tol, the transformation of the REC into HEX structure was also observed to be hindered in areas containing many elbows. In contrast, there would be very large grains and rapid phase transformation in areas of long-running parallel reconstruction lines (Figure 7d-f).

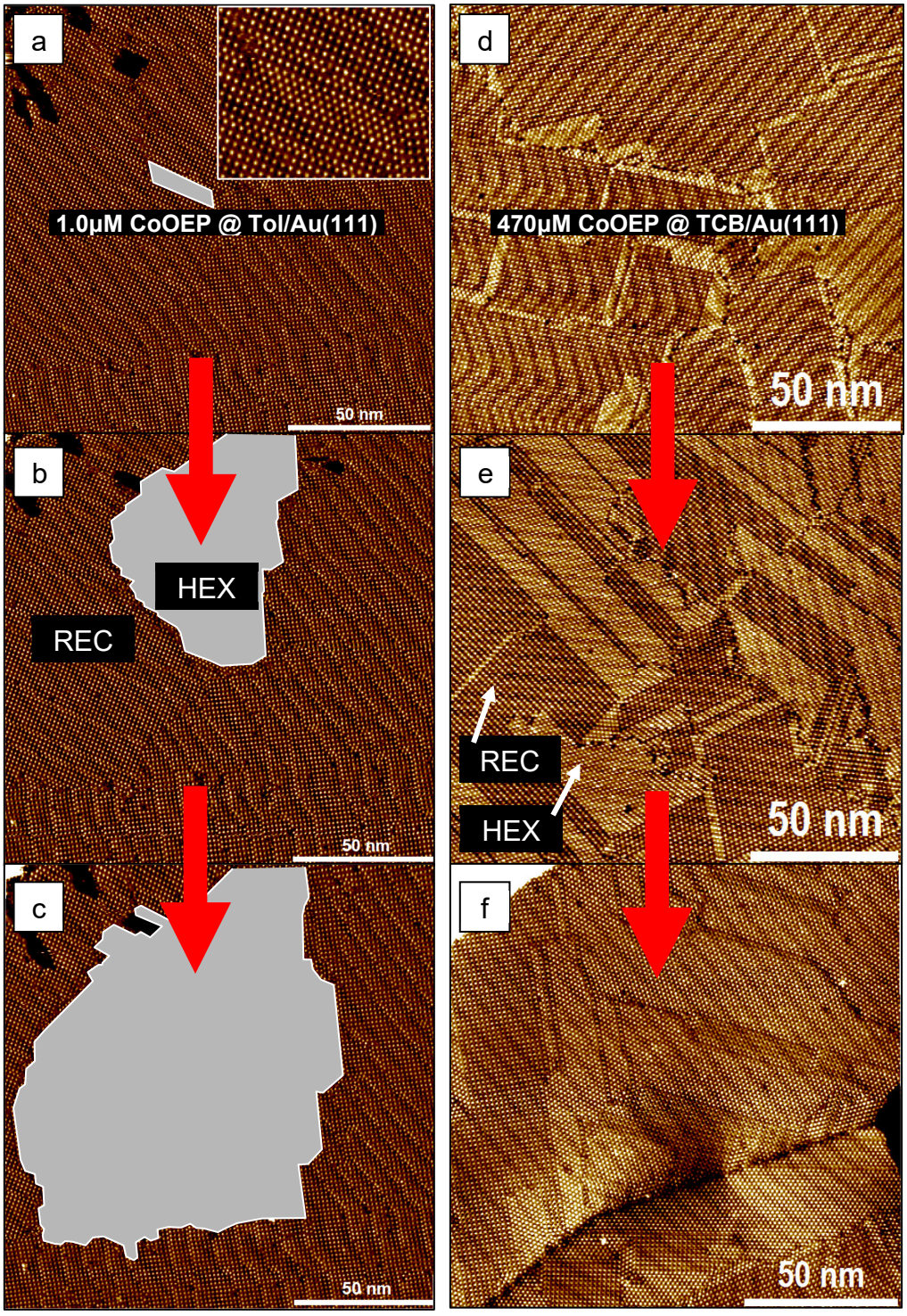

Figure 7. Series of images capturing the transformation of REC adlayer converting into HEX structure under solvents Tol (a-c) and TCB (d-f). The transition under 1 μM CoOEP in Tol is presented in sequential images resulting from continuously scanning the same region (a-c). Here a growing HEX grain highlighted in white, 2x magnification of grain shown in inset of (a). The time from initial introduction of solution to flow cell: t = 13 min (a), 15 min (b), 17 min (c). Due to the much slower dynamic in TCB, the images under 470 μM CoOEP in TCB (d-f) are of different scan regions under static solution: t = 1 hour (d), 18 hours (e), 44 hours (f). Scanning parameters: -0.4 V, 15 pA.

In order to better understand the role of the substrate in the incorporation of solvent, we calculated the adsorption energies of Tol and TCB on Au(111) and on HOPG. The results appear in Table 2. As can be seen from the Table, there is a roughly 1 order decrease in desorption rate of TCB from Au(111) over HOPG, but the corresponding ratio for toluene is two orders. We believe that it is this 358 factor is the primary reason that Tol incorporates into CoOEP on Au and not on HOPG.

Table 2. DFT calculated adsorption energies (eV) for solvents on Au(111) and C(0001). Also shown are the indicated ratios of the desorption rate constants.

Desorption Energy (eV)		
	Au	HOPG
TCB	-1.040	-0.976
Toluene	-0.882	-0.731
Ratio of Desorption Rate Arrhenius Factors		
TCB(HOPG)/TCB(Au)		12
Tol(Au)/TCB(Au)		470
Tol(HOPG)/TCB(HOPG)		14000
Tol(HOPG)/Tol(Au)		358

Dynamics, Kinetics, and Stability of Self-Assembly

The concentration of the solution in the diffusion layer in contact with the substrate is typically assumed to be equal to the concentration of the bulk solution, but this needs to be reconsidered when working with dilute compounds.[51] To combat the depletion of tectons in the diffusion layer during self-assembly, an STM flow cell system was developed to have dynamic control of solution flow (Figure 2). Unlike static solution cell studies, this flow cell design allows the system to be monitored by STM while providing the dynamic control of solvent and adsorbate concentration throughout the entire self-assembly process. With the help of this flow cell, we were able to (1) continuously replenish tectons to the diffusion layer for self-assembly at very low concentrations and (2) thin the diffusion layer thickness via flow across the surface. In this study, the volume of

the flow cell was initially filled within a minute (55 μL/min flow rate), and then the flow was decreased to replenish the cell every 5 minutes (5 μL/min flow rate). The STM tip was positioned in the cell to optimize flow of fresh solution in order to keep the concentration near the surface equal to the concentration of the bulk solution during the self-assembly.

Using this custom flow cell design, the early stages of assembled island nucleation and growth were captured and monitored using STM (Figure 8). Because the adlayer growth is dependent on the adsorbate concentration, dilute solutions were used to slow the assembly kinetics to the time scale of STM imaging (~minutes). While imaging a freshly annealed Au(111) substrate under air, a 0.25 μM solution of CoOEP in PhO was injected into the flow cell and across the surface. Islands were observed to nucleate on the Au(111) reconstruction lines, preferentially growing along and across neighboring rows, while growth was hindered by the 'herringbone' elbows of the reconstruction or any defects/contaminants on the surface.

Even at extremely low concentrations (~50 nM), given enough time and enough molecules in solution, the adlayer will reach full monolayer coverage. This is a testament to the extremely strong interaction between the porphyrin and Au(111).

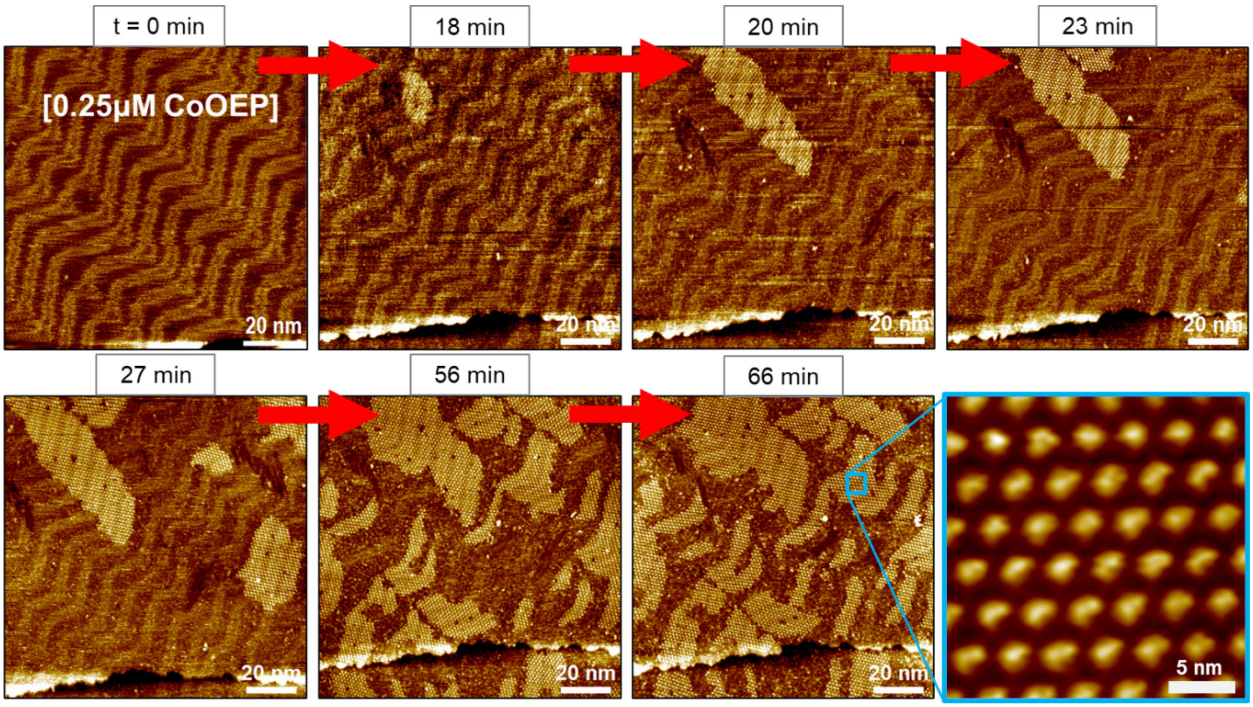

Figure 8. Real-time nucleation and growth of CoOEP islands at the PhO/Au(111) interface with constant 1 μM CoOEP solution flow captured by STM. Time indicated represents duration of flow from initial contact of solution with surface. Assembled islands appear to nucleate on reconstruction lines and growth is hindered by elbows in the reconstruction lines. Inset in blue box is a high-resolution image of the adlayer structure. Scanning parameters: -0.4 V, 15 pA.

Similar to platinum(II) octaethylporphyrin at the $HClO_4$/Au(111) interface,[52] the CoOEP adlayer here was found to stabilize the reconstruction of the Au(111) surface under all solvents studied. As time went on and solution was being pumped through the flow cell, areas of the Au(111) surface ***without*** CoOEP islands were observed to relax and lose the reconstruction. When running large volumes of low concentration solutions across the Au(111) surface, the solvent purity becomes pertinent. Contaminants could lift the Au(111) reconstruction or preferentially adsorb onto the surface and obstruct the self-assembly. Thus, the observed changes in reconstruction are likely due to fouling from minute amounts of impurities in solution interacting with the surface. This was particularly evident at low concentrations of porphyrin (<1 μM) where the adlayer growth was slowest. At higher concentration, the adlayer quickly grew to cover the entire Au(111) surface and was found to preserve the reconstruction, even after several days of being under solution (Figure

7f). Adsorption experiments spanning several days at very low concentrations would typically be spoiled by contamination of the Au(111) surface and partial adlayer coverage. So, to study the kinetics of self-assembly, the concentration of the adsorbate needed to be low enough to slow the formation time to allow imaging by STM, but high enough to combat the fouling effects of contaminants. We found this range of concentrations to be about 0.25 μM ~ 1 μM.

To study the kinetics of island formation, the coverage of the growing adlayer was measured as a function of time from the initial introduction of solution to the Au(111) surface (Figure 9a-d). To interpret this data, we used a modified Avrami equation proposed by Gualtieri[53] to model the kinetics of nucleation and growth. The nucleation expression of this model considers a Gaussian distribution of probability, and the growth expression is based on Avrami growth kinetics. Using this functional form to describe the coverage of a growing adlayer as a function of time, Equation 1 results.

$$M = \frac{1}{1+e^{-\left(\frac{t-a}{b}\right)}} * \left\{1 - e^{-(kt)^n}\right\} \qquad (1)$$

Here, M is fractional coverage of adlayer on the surface, k is the rate constant associated with island growth, n is the Avrami growth constant associated with the dimensionality of growth, a is the time delay for nucleation, b is the distribution of the nucleation probability with time. The self-assembly of CoOEP on Au(111) from Dec, PhO, and TCB were fit with this model; the fits were excellent. For example, Figure 9d shows the fit (broken line) in the case of PhO. Unfortunately, the fits are not unique. There is considerable cross-correlation between the values of *b*, *k*, and *n*. The *a* parameter, on the other hand, is reasonably independent of starting values for the fit and has small uncertainty. Rather than list extracted parameters (that are not unique) we instead provide in Table 3 the nucleation time parameter, *a*, and time required to reach 80% of a monolayer, Θ_{80}, after initial nucleation. When imaging the formation under Tol, issues of contaminant within the

solvent prevented collecting reliable data on the formation kinetics (possibly due to chemical leaching from the Teflon tubing, which was not observed in the other solvent).

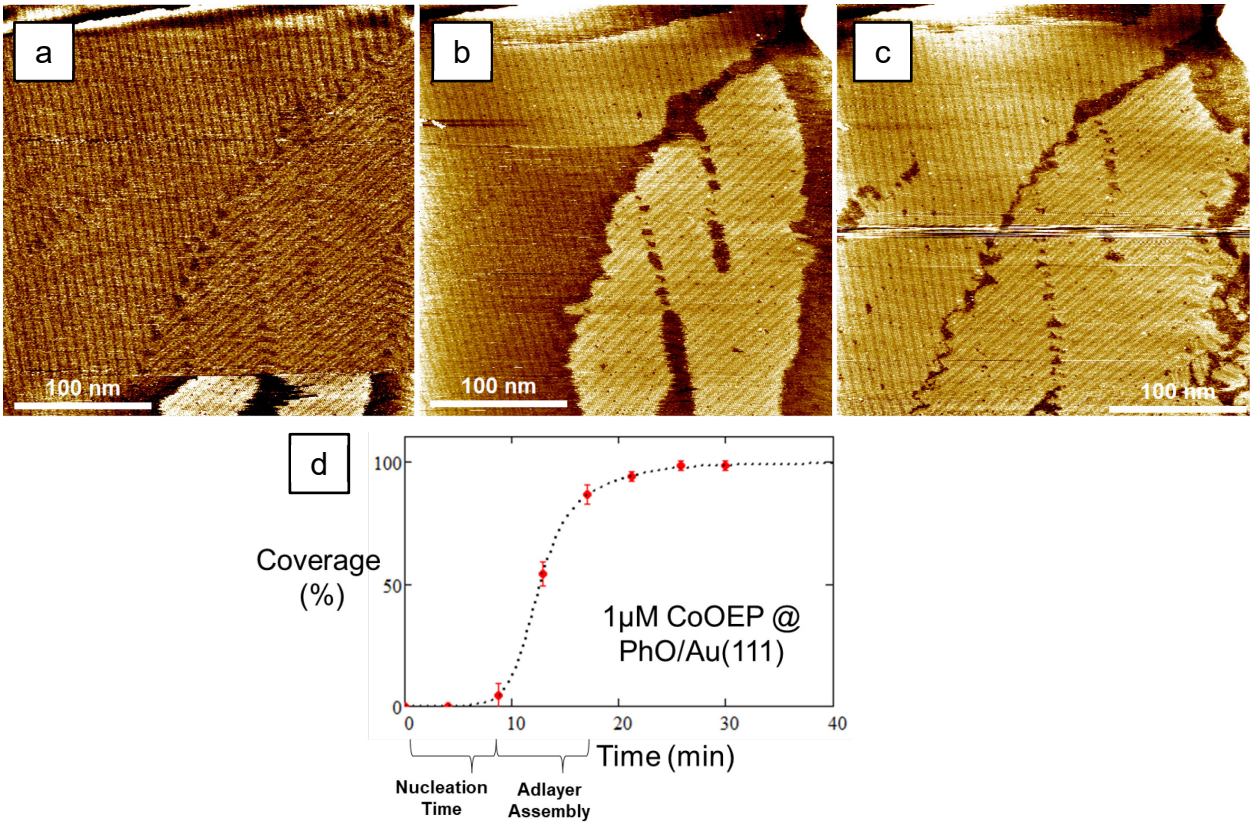

Figure 9. Sequence of images capturing the CoOEP adlayer formation at the PhO/Au(111) interface (a-c) collected at a rate of 4 minutes per frame. Fractional coverage of the assembled adlayer was measured as a function of time (d). Data are fit with Eq 1, and the extracted parameters for nucleation and growth are shown in Table 3. Reconstruction lines of Au(111) surface are seen as long running parallel rows as well as herringbone elbows. Because assembly of islands is dependent on surface diffusion of adsorbed molecules, growth along rows is fast but hindered by elbows in the reconstruction. Scanning parameters: -0.4 V, 15 pA.

Table 3. Parameters associated with the nucleation and growth of CoOEP on Au(111) from solvents PhO, Dec and TCB. The parameter a was taken from the modified Avrami equation.

Solvent	[CoOEP]	a (min)	Θ_{80}(min)
PhO	1.0 μM	12 ± 1	8 ± 1
Dec	1.0 μM	15 ± 1	5 ± 1
TCB	1.0 μM	5 ± 1	4 ± 1

It should be noted that non-specific adsorption or formation of amorphous agglomerates of adsorbate likely occur during the initial stages of the self-assembly process (evident in Figure 10), but the nucleation events of interest are those which seed the growth of the commensurate adlayer captured by STM. Though the modified Avarmi model provides reasonable fits to the experimental data, it is not based on the molecular mechanisms of self-assembly at the solution solid interface. No proper kinetic rate equation has been proposed for the island formation of non-covalent systems that truly reflects the mechanisms of the self-assembly process. It must be noted that one study monitored the formation kinetics of corrole derivatives at the EtOH/Au(111) interface; however, the adlayer structure was ambiguous and the growth was fit to a Langmuir function without physical justification.[54]

Adlayer formation was also monitored with solvents Tol, TCB, and Dec (Figures S5, S6, and 10, respectively). The characteristics of island growth under the solvents was notably different. The formation under Dec and Tol produced many nucleation sites and a monolayer with many grains, while larger grains were observed under PhO and TCB.

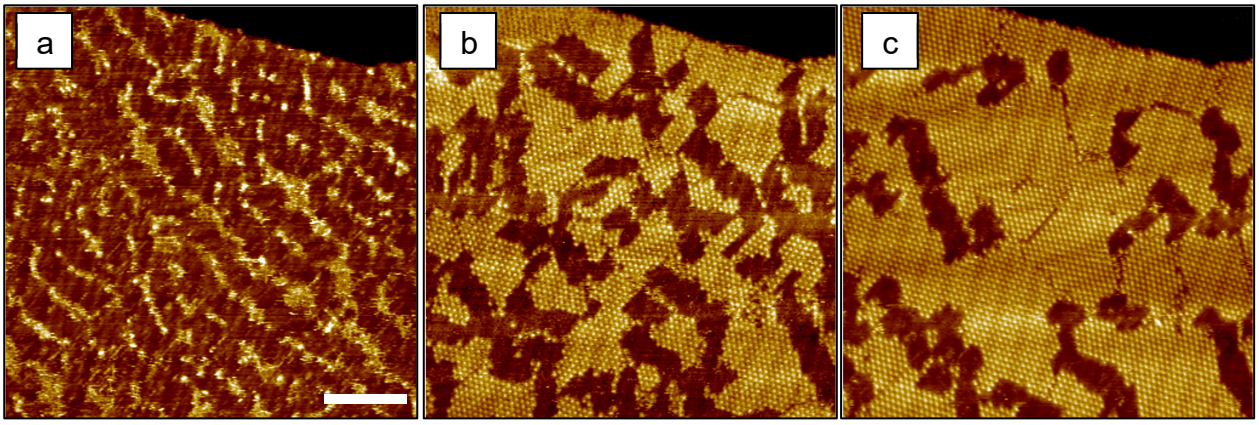

Figure 10. Self-assembly of 0.5 μM CoOEP in Dec on Au(111). Images are 9 min apart. Scale bar is 20 nm for all images. Scanning parameters: -0.4 V, 15 pA.

It has been shown that the STM scanning can influence adlayer nucleation and dissolution,[55-57] so it is important to consider tip effects when studying the kinetics of adlayer formation,

particularly during experiments with low solution concentration. In previous work on HOPG, it was found that STM imaging can assist in the dissolution of ordered islands and impede the formation of the monolayer. Therefore, it is important to maximize the scan area to minimize tip-adsorbate interaction and optimize solution flow to maintain a constant supply of adsorbate to the region of analysis. To confirm quality of data, regions around the initial scan area were imaged and inspected for variation in adlayer formation relative to the previously scanned area. To minimize the extent of tip influenced and diffusion limited self-assembly, (1) ideal solution flow must be maintained throughout experiment, (2) large scan areas should be imaged, and (3) regions surrounding the area of interest must be imaged to confirm uniform growth.

De Feyter[58,59] and Lee[60] have demonstrated that solution flow direction could affect the adlayer assembly, structure, and stability. However, effects due to the direction of solution flow with respect to the substate were not observed during these experiments.

An example of dramatic tip-influence on adlayer growth under slow solution flow is shown in (Figure 11). After monitoring the adlayer formation of a region, the scan size was increased, and the surrounding area was observed to grow only after the area was further scanned. Here, the tip-surface interaction appears to preferentially promote the assembly of islands within the scanned region. The data used to generate Table 3 did not exhibit differences between the region monitored during the adlayer formation and the surrounding areas.

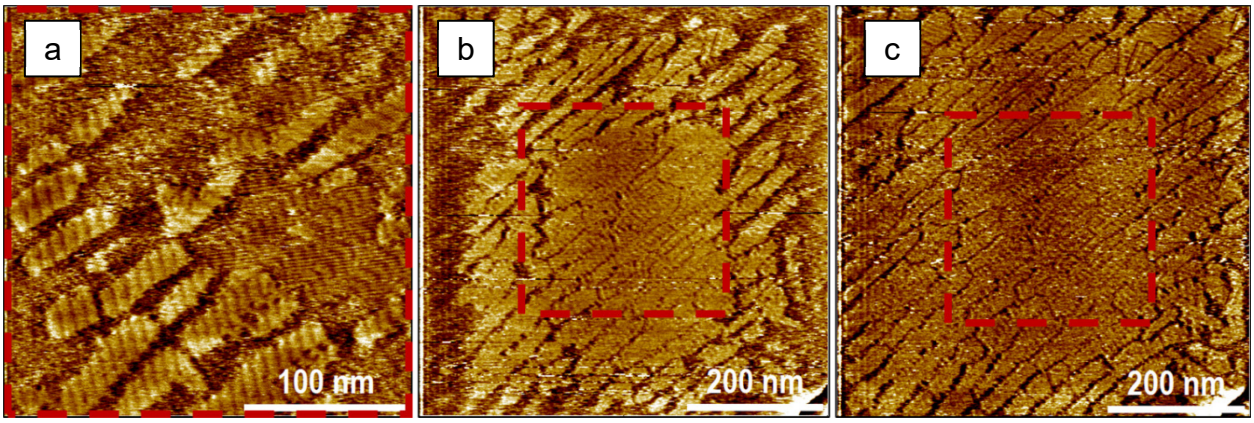

Figure 11. Example of tip-influenced adlayer formation. Series of images of slow flowing 0.5 µM CoOEP at Dec/Au(111). After adlayer formed in initial imaging region (250 nm x 250 nm) (a), scan area was increased (600 nm x 600 nm) (b-c). Scanning parameters: -0.4 V, 20 pA.

Substrate Effects on Self-Assembly, Au(111) vs HOPG

Adlayer formation is clearly dependent on the structure and chemistry of the substrate surface.[61] For example, Uemura *et al*[62] observed that the adsorbate-substrate interactions were the governing force driving the morphologies of fullerene adlayers on Au(111) and Pt(111). It is no surprise there is variation in the dynamics and energetics of self-assembly on Au(111) compared to HOPG. Aside from local defects in the surface structure, the graphite surface is uniform while the Au(111) reconstructed surface is innately energetically inhomogeneous.[63,64] CoOEP self-assembled islands appeared to nucleate non-specifically on HOPG and grew very rapidly. Adlayer formation on HOPG was readily reversible and the growing islands had dynamic and oscillating boundaries which allowed for dynamic rearrangement to form large uniform grains by Oswald ripening.

The exchange of adlayer-incorporated CoOEP molecules with solution has been previously studied, where the temperature-dependent desorption rates and desorption energies at the PhO/Au(111) interface were determined for molecules internal to islands.[65] To maintain a constant supply of molecules to exchange, the concentration of the solution was ~10^2 µM. It was found that the adlayer (similar to the reported HEX structure here) was kinetically bound below 100˚C.

The barrier for desorption was so great that a temperature of 135 °C was required to induce desorption over a period of hours, with a rate constant of 4.0×10^{-3} min^{-1}. The desorption of adlayer-incorporated CoOEP on Au(111) was compared to HOPG.[66] It was found that the calculated desorption rate from HOPG (2.2×10^{-1} min^{-1}) was two orders of magnitude greater than from Au(111). These observations agree well with what is reported in this current study, where CoOEP is much more strongly bound to Au(111) than HOPG. The combination of these studies broadly expands the understanding of the kinetics of self-assembly at the solution solid interface, and the critical role the substrate can play in the adlayer formation, energetics, and dynamics.

Due to the energetic variation in the Au(111) surface, it is expected that the diffusion of molecules across the surface, and in turn, the nucleation and growth would be inhomogeneous. Islands were observed to preferentially nucleate along the reconstruction lines. The growth of the islands was also greatly dependent on the nature of the gold surface, being hindered by the elbow of the reconstruction. When compared to the formation on HOPG, the molecules at the perimeter of growing islands on Au(111) were more energetically stabile and the growth of formed islands was not easily reversible, especially at high adlayer coverage. This led to the presence of many grains and defects within the adlayer structure on regions of herringbone elbows, and large grains atop areas with long running parallel reconstruction lines. On HOPG, an equilibrium between CoOEP in solution and an assembled adlayer was observed at a threshold concentration. On Au(111), however, the reaction heavily favored a complete assembled adlayer at all experimental conditions, even at extremely low concentrations studied (<0.1 μM).

Solvent-induced adlayer structure was also found to be different on Au and on HOPG. PhO, Dec, and Tol all formed only a HEX structure on HOPG, while TCB formed a very stable REC structure. Adsorption from extremely high CoOEP concentrations (~7 mM) in TCB formed grains

of both REC and HEX on HOPG, and the amount of HEX increased with time while REC decreased. On Au(111) however, a very slow conversion (~10^2 minutes) from REC to HEX was observed at lower concentrations (~500 μM) under TCB. Surprisingly, a solvent-incorporated REC structure was observed under Tol on Au(111) at low concentrations (<1 μM), but not on HOPG at any concentration up to the solubility limit of the CoOEP. A conversion from the initially formed REC structure to HEX occurred on the order of ~10 minutes. This variance in conversion time and concentration dependance of the adlayer structure alludes to the difference in the energetic contributions of the solvent in the assembly process. Assuming that the adlayer forms a commensurate structure atop the substrate, the estimated unit cell parameters are also substrate dependent. The HEX structure on Au(111) covers a slightly larger area than on HOPG. The REC on Au(111) contains two CoOEP but only one CoOEP on HOPG. As in the HEX case, the unit area per molecule for the REC structure is slightly larger on Au(111), but contains two CoOEP per unit cell on both substrates.

CONCLUSION

Self-assembly of CoOEP at the solution/Au(111) interface at room temperature was found to be kinetically driven and not reversible. Solvent was found to play a significant role in each step of the self-assembly process, from adlayer structure and stability to adlayer formation kinetics.

Through the use of a custom STM flow cell and the experimental approach demonstrated here, characteristic kinetic parameters of self-assembly have been extracted. Unlike other studies which used static solution cells, this setup allows for monitoring early (and late) self-assembly with molecular resolution, under volatile solvent, and at extremely low concentrations while minimizing mass-transfer diffusion effects and preventing depletion of the solution of tectons during the adsorption process.

Parameters associated with the nucleation and growth of the observed monolayer were extracted by fitting the fractional coverage of self-assembled adlayer with a modified Avrami equation. The rate of formation from TCB was found to be an order of magnitude faster than from Dec and PhO solvents. Formation kinetics from Tol were not analyzed due to convolution of data from contaminant in solvent at high flow rates and low CoOEP concentrations. Both TCB and Tol solvents were found to incorporate into the adlayer structure. This is the first report to observe the co-adsorption of Tol into a self-assembled adlayer at the solution/solid interface.

It was found that the Au(111) surface plays a much more dramatic role in the adlayer formation, kinetics, and stability than HOPG. On HOPG, by holding the solution concentration above a solvent-dependent threshold, the adlayer could be formed within ~15 minutes. Or by lowering the solution concentration below the threshold, the adlayer can be dissolved away within minutes (for TCB and Tol). Under PhO and Dec, partial adlayer coverage was still observed after hours of being under pure solvent. These residual islands were observed to be eroded away by the scanning of the STM tip.

On Au(111), the adlayer formed even at extremely low concentrations (<0.1uM) for all solvents within ~10 minutes of nucleation. Even under pure flowing solvent, the formed adlayer remained very stable and significant dissolution was not observed. Solvent incorporation was observed for only TCB on HOPG, but for both TCB and Tol on Au(111). The concentration of CoOEP in solution needed to transition from the TCB-incorporated to solvent-free structure was a magnitude greater on HOPG (~7 mM) than on Au(111) (~0.5 mM). This suggests that the incorporated solvent is in dynamic equilibrium with solution, and exchanges from the surface to solution at much greater rates than the CoOEP. These observations hint at the relative interactions of the different systems and show that the Au(111)-solvent and Au(111)-CoOEP interactions are greater (compared to

HOPG) and contribute to the balance of the self-assembly process. In short, intermolecular interactions within the adlayer (adsorbate + solvent for REC) dominate the self-assembly on HOPG, while the adsorbate-substrate contribution is more significant on Au(111)

This study not only provides an experimental framework to extracting qualitative information about the thermodynamics and kinetics of self-assembly at the solution/solid interface, but also provides an approach to understanding the mechanisms and energetics of the self-assembly process.

ASSOCIATED CONTENT

The Supporting Information is available free of charge at https://pubs.acs.org/XXXXXXX. Information is provided concerning the free energy calculations and optimization results. Also provided are selected STM images.

AUTHOR INFORMATION

Corresponding Author

K. W. Hipps − Department of Chemistry and Materials Science and Engineering Program, Washington State University, Pullman, Washington, 99163-4630, United States; orcid.org/0000-0002-5944-5114; Email: hipps@wsu.edu

Authors

Kirill Gurdumov − Department of Chemistry and Materials Science and Engineering Program, Washington State University, Pullman, Washington, 99163-4630, United States; orcid.org/0000-0001-5692-4825

Ursula Mazur − Department of Chemistry and Materials Science and Engineering Program, Washington State University, Pullman, Washington 99163-4630, United States; orcid.org/0000-0002-3471-4883

Funding Sources

This work was supported by the US National Science Foundation in the form of grant CHE1807225.

Notes

The authors declare no competing financial interest

ACKNOWLEDGMENT

This work was supported by the US National Science Foundation in the form of grant CHE1807225.

REFERENCES

[1] Mali, K. S.; Adisoejoso, J.; Ghijsens, E.; De Cat, I.; De Feyter, S. Exploring the complexity of supramolecular interactions for patterning at the liquid–solid interface. *Acc. Chem. Res.* **2012**, *45*, 1309 – 1320.

[2] Hipps, K. W.; Mazur, U. Kinetic and Thermodynamic Control in Porphyrin and Phthalocyanine Self-Assembled Monolayers. *Langmuir*, **2018**, *34*, 3 – 17.

[3] Rana, S.; Johnson, K. N.; Gurdumov, K.; Mazur, U.; Hipps, K. W. Scanning Tunneling Microscopy Reveals Surface Diffusion of Single Double-Decker Phthalocyanine Molecules at the Solution/Solid Interface *J. Phys. Chem. C* **2022**, *126*, 4140 – 4149.

[4] Gutzler, R.; Cardenas, L.; Rosei, F. Kinetics and thermodynamics in surface-confined molecular self-assembly *Chem. Sci.*, **2011**, *2*, 2290 – 2300.

[5] Mamdouh, W.; Uji-i, H.; Ladislaw, J. S.; Dulcey, A. E.; Percec, V.; De Schryver, F. C.; De Feyter, S. Solvent Controlled Self-Assembly at the Liquid-Solid Interface Revealed by STM. *J. Am. Chem. Soc.* **2006**, *128*, 317– 325.

[6] Yang, Y.; Wang, C. Solvent effects on two-dimensional molecular self-assemblies investigated by using scanning tunneling microscopy. *Curr. Opin. Colloid Interface Sci.*, **2009**, *14*, 135.

[7] Zhao, M.; Deng, K.; Jiang, P.; Xie, S. S.; Fichou, D.; Jiang, C. Binary-Component Self-Assembled Monolayer Comprising Tetrathiafulvalene and n-Tetradecane Molecules with Periodic Ordered Phase Separation Structures on a Highly Oriented Pyrolytic Graphite Surface J. Phys. Chem. C **2010**, *114*, 1646 – 1650.

[8] Marie, C.; Silly, F.; Tortech, L.; Müllen, K.; Fichou, D. Tuning the Packing Density of 2D Supramolecular Self-Assemblies at the Solid-Liquid Interface Using Variable Temperature. *ACS Nano* **2010**, *4*, 1288 – 1292.

[9] Maeda, M.; Nakayama, R.; De Feyter, S.; Tobe, Y.; Tahara, K. Hierarchical two-dimensional molecular assembly through dynamic combination of conformational states at the liquid/solid interface *Chem. Sci.***, 2020**, *11*, 9254 – 9261.

[10] English, W. A.; Hipps, K.W. Stability of a Surface Adlayer at Elevated Temperature: Coronene and Heptanoic Acid on Au(111). *J. Phys. Chem. C*, **2008**; 112; 2026-2031.

[11] Lackinger, M.; Griessl, S.; Heckl, W. M.; Hietschold, M.; Flynn, G. W. Self-Assembly of Trimesic Acid at the Liquid– Solid Interface a Study of Solvent-Induced Polymorphism. *Langmuir* **2005**, *21*, 4984 – 4988.

[12] Jahanbekam, A.; Vorpahl, S.; Mazur, U.; Hipps, K. W. Temperature Stability of Three Commensurate Surface Structures of Coronene Adsorbed on Au(111) from Hepatanoic Acid in the 10ºC to 60ºC Range. *J. Phys. Chem. C* **2013**, *117,* 2914-2919.

[13] Gyarfas, B. J.; Wiggins, B.; Zosel, M.; Hipps, K. W. Supramolecular Structures of Coronene and Alkane Acids at the Au(111)-Solution Interface: A Scanning Tunneling Microscopy Study. *Langmuir* **2005**, *21*, 919 – 923.

[14] Wu, J.; Li, J.; Dong, M.; Miao, K.; Miao, X.; Wu, Y.; Deng, W. Solvent Effect on Host–Guest Two-Dimensional Self-Assembly Mediated by Halogen Bonding. *J. Phys. Chem. C* **2018**, *122*, 22597 – 22604.

[15] S. Lee, S.; Hirsch, B. E.; Liu, Y.; Dobscha, J. R.; Burke, D. W.; Tait, S. L.; Flood, A. H. Multifunctional Tricarbazolo Triazolophane Macrocycles: One-Pot Preparation, Anion Binding, and Hierarchical Self-Organization of Multilayers. *Chem. Eur. J.* **2016**, *22*, 560 – 569.

[16] Hu, Y.; Lee, S.-L.; Deng, W. L. Structural Diversity and Phase Transition Control via Kinetics and Thermodynamics in Mixed Solvents: Two-Dimensional Self-Assembly at the Liquid/Solid Interface. *J. Phys. Chem. C* **2020**, *124*, 27148 – 27157.

[17] Hipps, K. W.; Lu, X.; Wang, X.D.; Mazur, U. Metal d-orbital Occupation Dependent Images in the Scanning Tunneling Microscopy of Metal Phthalocyanines. *J. Phys. Chem.* **1996**, *100***,** 11207-11210..

[18] Suzuki, Y.; Enoki, H.; Akiba, E. Observation of HOPG by STM and contact AFM in various gas atmospheres under pressures up to 1.1 MPa *Ultramicroscopy* **2005**, *104*, 226 – 232.

[19] Wilms, M.; Kruft, M.; Bermes, G.; Wandelt, K. A new and sophisticated electrochemical scanning tunneling microscope design for the investigation of potentiodynamic processes *Rev. Sci. Instrum.* **1999**, *70*, 3641 – 3650.

[20] Gurdumov, K.; Mazur, U.; Hipps, K.W. Self-Assembly and Stability Through Concentration Control at the solution/HOPG Interface. *J. Phys. Chem. C* **2022**, *126*, 12916 – 12927.

[21] Wang, Y.; Milao, X.; Deng, W. Halogen Bonds Fabricate 2D Molecular Self-Assembled Nanostructures by Scanning Tunneling Microscopy *Crystals* **2020**, *10*, 1057.

[22] Koudia, M.; Abel, M.; Maurel, C.; Bliek, A.; Catalin, D.; Mossoyan, M.; Mossoyan, J.-C.; Porte, L. Influence of Chlorine Substitution on the Self-Assembly of Zinc Phthalocyanine *J. Phys. Chem. B* **2006**, *110*, 10058 – 10062.

[23] Greulich, K.; Belser, A.; Basova, T.; Chasse, T.; Peisert, H. Interfaces between Different Iron Phthalocyanines and Au(111): Influence of the Fluorination on Structure and Interfacial Interactions *J. Phys. Chem. C* **2022**, *126*, 716 –727.

[24] Kresse, G.; Furthmüller, J. Efficiency of Ab-Initio Total Energy Calculations for Metals and Semiconductors Using a Plane-Wave Basis Set. *Comput. Mater. Sci.* **1996**, *6*, 15 – 50.

[25] Kresse, G.; Hafner, J. Ab Initito Molecular Dynamics for Liquid Metals. *Phys. Rev. B* **1993**, *47*, 558 – 561.

[26] Kresse, G.; Joubert, D. From Ultrasoft Pseudopotentials to the Projector Augmented-Wave Method. *Phys. Rev. B* **1999**, *59*, 1758.

[27] Blöchl, P. E. Projector Augmented-Wave Method. *Phys. Rev. B* **1994**, *50*, 17953.

[28] Klimeš, J.; Bowler, D. R.; Michaelides, A. Van der Waals Density Functionals Applied to Solids. *Phys. Rev. B* **2011**, *83*, 195131.

[29] Becke, A. D. Density-Functional Exchange-Energy Approximation with Correct Asymptotic Behavior. *Phys. Rev. A* **1988**, *38*, 3098.

[30] Perdew, J. P.; Burke, K.; Ernzerhof, M. Generalized Gradient Approximation Made Simple. *Phys. Rev. Lett.* **1996**, *77* (18), 3865. Perdew, J. P.; Burke, K.; Ernzerhof, M. Generalized Gradient Approximation Made Simple. *Phys. Rev. Lett.* **1996**, *77*, 3865.

[31] Nandi, G.; Chilukuri, B.; Hipps, K.W.; Mazur, U. Surface directed reversible imidazole ligation to nickel(II) octaethylporphyrin at the solution/solid interface: a single molecule level study. *Phys. Chem. Chem. Phys.* **2016,** *18,* 20819 – 20829.

[32] Jahanbekam, A.; Chilukuri, B.; Mazur, U.; Hipps, K. W. Kinetically Trapped Two-Component Self-Assembled Adlayer. *J. Phys. Chem. C* **2015**, *119,* 25364 – 25376.

[33] Chilukuri, B.; Mazur, U.; Hipps, K. W. Effect of Dispersion on Surface Interactions of Cobalt(II) Octaethylporphyrin Monolayer on Au(111) and HOPG(0001) Substrates: A Comparative First Principles Study. *Phys. Chem. Chem. Phys.* **2014**, *16*, 14096 – 14107.

[34] Borders, B.; Adinehnia, M.; Chilukuri, B.; Ruf, M.; Hipps, K. W.; Mazur, U. Tuning the Optoelectronic Characteristics of Ionic Organic Crystalline Assemblies. *J. Mater. Chem. C* **2018**, *6*, 4041 – 4056.

[35] Adinehnia, M.; Borders, B.; Ruf, M.; Chilukuri, B.; Hipps, K. W.; Mazur, U. Comprehensive Structure–Function Correlation of Photoactive Ionic π-Conjugated Supermolecular Assemblies: An Experimental and Computational Study. *J. Mater. Chem. C* **2016**, *4*, 10223 – 10239.

[36] Zhang, Y. C.; Chilukuri, B.; Hanson, T. B.; Heiden, Z. M.; Lee, D. Y. Connecting Solution-Phase to Single-Molecule Properties of Ni(Salophen). *J. Phys. Chem. Lett.* **2019**, *10*, 3525 – 3530.

[37] Hanke, F.; Björk, J. Structure and local reactivity of the Au(111) surface reconstruction. *Phys. Rev. B* **2013**, *87*, 235422

[38] Scudiero, L.; Barlow, D. E.; Hipps, K. W. Scanning Tunneling Microscopy, Orbital-Mediated Tunneling Spectroscopy, and Ultraviolet Photoelectron Spectroscopy of Nickel(II) Octaethylporphyrin Deposited from Vapor. *J. Phys. Chem. B* **2002**, *106*, 996 −1003.

[39] Ferreira, Q.; Bragança, A.; Moura, N.; Faustino, M.; Alcácer, L.; Morgado, J. Dynamics of porphyrin adsorption on highly oriented pyrolytic graphite monitored by scanning tunnelling microscopy at the liquid/solid interface. *Appl. Surf. Sci.* **2013**, *273*, 220 – 225.

[40] Cousty, J.; Marchenko, A. Substrate-induced freezing of alkane monolayers adsorbed on Au(111) dependant on the alkane/gold misfit *Sur. Sci.* **2002**, *520*, 128 – 136.

[41] Marchenko, O.; Cousty, J. Molecule Length-Induced Reentrant Self-Organization of Alkanes in Monolayers Adsorbed on Au(111). *Phys. Rev. Lett.* **2000**, *84*, 5363.

[42] Marchenko, A.; Lukyanets, S.; Cousty, J. Adsorption of alkanes on Au(111): Possible origin of STM contrast at the liquid/solid interface *Phys. Rev. B* **2002**, *65*, 045414.

[43] Kim, Y.; Kim, Y.; Park, J. Y. Restructuring of Porphyrin Networks Driven by Self-Assembled Octanoic Acid Monolayer on Au(111). *Langmuir* **2020**, *36*, 3792 – 3797.

[44] Noll, J. D.; Van Patten, P.G.; Nicholson, M.A.; Booksh, K.; Myrick, M.L. Flow injection system for the scanning tunneling microscope *Rev. Sci. Instrum.*, **1995**, *66*, 4150.

[45] Lay, M. D.; Sorenson, T. A.; Stickney, J. L. High-Resolution Electrochemical Scanning Tunneling Microscopy (EC-STM) Flow-Cell Studies *J. Phys. Chem. B* **2003**, *107*, 10598 – 10602.

[46] Keller, T. J.; Bahr, J.; Gratzfeld, K.; Schönfelder, N.; Majewski, M. A.; Stępień, M.; Höger, S.; Jester, S.-S. *Beilstein J. Org. Chem.* **2019,** *15,* 1848 – 1855.

[47] Iritani, K.; Takeda, H.; Kather, M.; Yokoi, M.; Moeglen, M.; Ikeda, M.; Otsubo, Y.; Ozawa, Y.; Tahara, K.; Hirose, K.; De Feyter, S.; Tobe, Y. Electrostatically Driven Guest Binding in Self-

Assembled Molecular Network of Hexagonal Pyridine Macrocycle at the Liquid/Solid Interface: Symmetry Breaking Induced by Coadsorbed Solvent Molecules. *Langmuir* **2019**, *35*, 15051 – 15062.

[48] Cui, D.; MacLeod, J. M.; Ebrahimi, M.; Rosei, F. Selective binding in different adsorption sites of a 2D covalent organic framework *CrystEngComm*, **2017**, *19*, 4927 – 4932.

[49] Nangia, A. Pseudopolymorph: Retain This Widely Accepted Term. *Crystal Growth & Design*, **2006**, *6*, 2-4.

[50] Wang, Y.; Xu,H.; Wang, H.; Li, S.; Gan, W.; Yuan, Q. Temperature dependent 2D self-assembled motif transition of copper–phthalocyanine derivates at air/HOPG interface: an STM study. *RSC Adv.* **2014**, *4*, 20256 – 20261.

[51] Jung, L. S.; Campbell, C. T. Sticking Probabilities in Adsorption from Liquid Solutions: Alkylthiols on Gold. *Phys. Rev. Lett.* 2000, 84, 5164– 5167, DOI: 10.1103/PhysRevLett.84.5164

[52] Yoshimoto, S.; Yasunishi, S.; Kawamoto, T. Effect of the Formation of Highly Ordered Platinum(II) Octaethylporphyrin Adlayer on the Surface Reconstruction of Gold and Supramolecular Assembly of Fullerenes. *J. Phys. Chem. C* **2014**, *118*, 29880 – 29886.

[53] Gualtieri, A. F. Synthesis of sodium zeolites from a natural halloysite. *Phys. Chem. Minerals* **2001**, *28*, 719-728.

[54] Bonanni, B.; Fanfoni, M.; Lacal, M.; Sgarlata, A.; Caroleo, F.; Paolesse, R.; Goletti C. Growth of Corrole Films from Solution: A Nanometer-Scale Study at the Real Solid–Liquid Interface *J. Phys. Chem. C* **2021**, *125*, 11540 – 11547.

[55] Reynaerts, R.; Mali, K. S.; De Feyter, S. Growth of a self-assembled monolayer decoupled from the substrate: nucleation on-command using buffer layers. *Beilstein J. Nanotechnol.* **2020,** *11,* 1291 – 1302.

[56] Rozbořil, F.; Ošťádal, I.; Sobotík, P.; Kocán, P. Self-Assembly of a Two-Dimensional Molecular Layer in a Nonhomogeneous Electric Field: Kinetic Monte Carlo Simulations. *Phys. Rev. E: Stat. Phys., Plasmas, Fluids, Relat. Interdiscip. Top.* **2019**, *99*, 032110.

[57] Coenen, M.J.J.; Khoury, T.; Crossley, M.J.; Hendriksen, B.L.M.; Elemans, J.A.A.W.; Speller, S. Nanostructuring of self-assembled porphyrin networks at a solid/liquid interface: Local manipulation under global control. *Chem. Phys. Chem.* **2014**, *15*, 3484.

[58] Lee, S. L.; Yuan, Z.; Chen, L.; Mali, K. S.; Mullen, K.; De Feyter, S. Forced To Align: Flow-Induced Long-Range Alignment of Hierarchical Molecular Assemblies from 2D to 3D. *J. Am. Chem. Soc.* **2014**, *136*, 11, 4117–4120.

[59] Lee, S. L.; Yuan, Z.; Chen, L.; Mali, K. S.; Mullen, K.; De Feyter, S. Flow-Assisted 2D Polymorph Selection: Stabilizing Metastable Monolayers at the Liquid–Solid Interface. J. Am. Chem. Soc. **2014**, *136*, 21, 7595–7598.

[60] Hu, Y.; Zeng, X.; Sahare, S.; Xie, R. B.; Lee, S. L. Flow-induced-crystallization: tailoring host–guest supramolecular co-assemblies at the liquid–solid interface. Nanoscale Adv., **2022**, *4*, 3524-3530.

[61] De Yoreo, J., Vekilov, P. *Rev. in Mineralogy and Geochemistry* **2003**, *54*, 57 – 93.

[62] Uemura, S.; Sakata, M.; Hirayama, C.; Kunitake, M. Fullerene Adlayers on Various Single-Crystal Metal Surfaces Prepared by Transfer from L Films. *Langmuir* **2004**, *20*, 9198 – 9201.

[63] Narasimhan, S.; Vanderbilt, D. Stress Domains and the Herringbone Reconstruction on Au(111). *Phys. Rev. Letters* **1992**, *69*, 1564 – 1567.

[64] Hanke, F.; Björk, J. Structure and Local Reactivity of the Au(111) Surface Reconstruction. *Phys Rev B* **2013**, *87*, 235422.

[65] Bhattarai, A.; Mazur, U.; Hipps, K. W. A Single Molecule Level Study of the Temperature-Dependent Kinetics for the Formation of Metal Porphyrin Monolayers on Au(111) from Solution. *J. Am. Chem. Soc.* **2014**, *136*, 2141 – 2148.

[66] Bhattarai, A.; Mazur, U.; Hipps, K. W. Desorption Kinetics and Activation Energy for Cobalt Octaethylporphyrin from Graphite at the Phenyloctane Solution–Graphite Interface: An STM Study. *J. Phys. Chem. C* **2015**, *119*, 9386 – 9394.